Available online at www.sciencedirect.com
SCIENCE DIRECT
Fluid Phase Equilibria 232 (2005) 136–148
FLUID PHASE EQUILIBRIA
www.elsevier.com/locate/fluid

Simulation of 1-alkene and *n*-alkane binary vapour–liquid equilibrium using different united-atom transferable force fields

Tyrone J. McKnight [a], Thijs J.H. Vlugt [b], Deresh Ramjugernath [a,*], Maciej Starzak [a], Peter Ahlström [c], Kim Bolton [c]

[a] *School of Chemical Engineering, University of KwaZulu-Natal, Durban 4041, South Africa*
[b] *Condensed Matter and Interfaces, Utrecht University, P.O. Box 80.000, 3508 TA Utrecht, The Netherlands*
[c] *School of Engineering, University College of Borås, SE-501 90 Borås, Sweden*

Received 28 May 2004; received in revised form 14 March 2005; accepted 15 March 2005
Available online 25 April 2005

Abstract

The configurational-bias Monte Carlo method in the Gibbs ensemble, using the NERD, TraPPE and Spyriouni et al. 1-alkene force fields, was used to simulate phase equilibrium data for the ethane + propene, 1-hexene + *n*-octane, *n*-dodecane + 1-octadecene, propene + 1-butene and 1-butene + 1-hexene binary mixtures. The NERD force field yields *P–x–y* data that are in better agreement with measured experimental data than those obtained from the TraPPE force field for alkane + 1-alkene and 1-alkene + 1-alkene mixtures that are comprised of short chain molecules. Both of these force fields yield results that agree with experimental data for binary mixtures consisting of long chain molecules. The Spyriouni et al. 1-alkene force field also yields *P–x–y* data for the 1-alkene + 1-alkene mixtures that agrees well with experiment data, but the *n*-alkane parameters from the SA1 force field yield inaccurate coexistence densities for *n*-alkanes shorter than *n*-dodecane and hence are not transferable to these shorter *n*-alkanes. All force fields yield *x–y* diagrams that are in very good agreement with experimental data for the mixtures studied. It was found that assuming ideal solution behaviour and linear additivity of the species molar volumes provided a means to reasonably estimate the starting conditions for the simulations. It is also shown how the results of a Gibbs ensemble simulation and a reaction Gibbs ensemble simulation may be easily interchanged by using a simple calculation procedure without the need for a full calculation, and that the reaction Gibbs ensemble in general compromises the true molar composition predicted by a force field to achieve a shift in the phase diagram.

Keywords: Molecular simulation; Vapour–liquid equilibria; Chemical potential; Vapour pressure; Mixture

1. Introduction

Binary vapour–liquid equilibrium (VLE) data are vital for the design of industrial separation equipment [1]. Molecular simulation offers a promising alternative means to obtain the VLE efficiently and cost effectively [2,3].

The development of configurational-bias Monte Carlo methods (CBMC) [4–8] in the Gibbs ensemble [9–11] has made it computationally feasible to simulate VLE for hydrocarbon mixtures. In addition, several transferable united-atom force fields have emerged recently such as the TraPPE [12–16], NERD [17–19], Spyriouni et al. olefin force field [20] and the *n*-alkane force field of Errington and Panagiotopoulos [21]. These force fields have made it possible to simulate a wide range of compounds, as well as mixtures that belong to certain homologous series of chemicals, without having to parameterize force fields for individual chemical compounds. Mixtures of *n*-alkanes have been studied using the TraPPE [22–25] and NERD force fields [26] as well as the Buckingham exp-6 potential force field of Errington and Panagiotopoulos [27]. More recently, anisotropic united-atom force fields have also been parameterized for the simulation of *n*-alkanes [28], branched alkanes [29] and 1-alkenes, 2-alkenes, isobutene and 1,3-butadiene [30]. These force fields have also been applied to

* Corresponding author. Tel.: +27 31 2603128; fax: +27 31 2601118.
E-mail address: ramjuger@ukzn.ac.za (D. Ramjugernath).

0378-3812/$ – see front matter © 2005 Elsevier B.V. All rights reserved.
doi:10.1016/j.fluid.2005.03.021

the simulation of *n*-alkanes and 1-alkene mixtures in zeolites [31,32].

1-Alkenes (α-olefins) are an important class of compounds that find wide application in industrial processes [33,34], and knowledge of their phase behaviour is vital for equipment design. In spite of this, there have been only a limited number of simulation studies of 1-alkene mixtures [19,35–37].

In this work we present results from CBMC Gibbs ensemble simulations for three *n*-alkane + 1-alkene mixtures (ethane + propene, 1-hexene + *n*-octane, *n*-dodecane + 1-octadecene) and two 1-alkene + 1-alkene mixtures (propene + 1-butene and 1-butene + 1-hexene). The mixtures investigated were chosen since they are systems for which experimental binary VLE data are available [38], and are representative of the types of mixtures which can be encountered in industrial separation operations such as petroleum refining [39], sub-atmospheric fractional distillation of petroleum [40], and in the synthetic chemical industry [41,42]. The TraPPE, NERD and the Spyriouni et al. α-olefin force fields were used for these simulations.

2. Force fields

The NERD, TraPPE and 1-alkene force field of Spyriouni et al. (SA1) were used because these force fields have been shown to reproduce experimental pure component phase equilibrium data reasonably well [12,15,17,19,20]. Also, these force fields were developed using different approaches for describing the intramolecular geometries and different thermophysical properties were targeted when optimizing the intermolecular potential energy parameters. The intermolecular interactions have been shown previously to play a dominant role in determining the pure component phase equilibrium properties [4,43]. The SA1 force field has fixed bond lengths and bond angles but flexible torsional angles; the TraPPE force field has constant bond lengths but flexible bond angles and torsional angles; and the NERD force field has flexible bond lengths, bond angles and torsional angles. In addition, the parameterization of the Lennard–Jones size (σ) and energy (ε) parameters for the SA1 force field differed to that of the NERD and TraPPE force fields. Specifically, when fitting the Lennard–Jones parameters for the SA1 force field, emphasis was placed on the experimental vapour pressures, while fitting of the NERD and TraPPE force fields focused on reproducing the experimental saturated liquid densities, critical temperatures and critical densities. It is therefore important to examine whether these differences will significantly affect the simulated phase diagrams of the mixtures studied here.

The selected force fields thus do not treat the carbon and hydrogen atoms explicitly, but treat the $-CH_3$, $-CH_2-$ and $-CH-$ groups in the hydrocarbon chain as single sites. These united-atom models thus assume that explicit treatment of the hydrogen atoms, which increases the computational requirements considerably, is not necessary. Instead the important effects of the hydrogen atoms, such as in giving a certain volume to each site, is implicitly taken into account via the force field parameters described below. As pointed out by Chen and Siepmann [14], the united-atom approximation reduces CPU calculation time by approximately one order of magnitude without significantly lowering the accuracy of the simulated phase equilibrium properties.

Recently developed anisotropic united-atom (AUA) force fields have also been shown to reproduce the pure component phase equilibrium data well [28–32]. The results for 1-alkenes have also shown that while the TraPPE-UA force field gives slightly better liquid density results, the AUA4 force field gives superior vapour pressure predictions [32]. It was the objective of this work, however, to use the NERD, TraPPE and Spyriouni et al. UA force fields only to establish how these recently developed UA force fields compare in predicting binary VLE for *n*-alkane + 1-alkene mixtures and to permit a comparison of how the different parameterization targets (vapour pressures or liquid densities and critical properties) affect the *P*–*x*–*y* and *x*–*y* diagrams for the mixtures.

All of the force fields studied here, use a cosine series arising from the work of Jorgensen et al. [45] to describe the torsional potential between four consecutive sites in the hydrocarbon chain:

$$U_{\text{tors}} = c_0 + c_1(1 + \cos\phi) + c_2(1 - \cos 2\phi) + c_3(1 + \cos 3\phi) \quad (1)$$

where ϕ is the torsional angle and c_0, c_1, c_2 and c_3 are constants which, together with other parameters, are listed in Table 1. The torsional angle is defined as 0.0° in the *cis* conformation for all torsions. The bond angles for the TraPPE and NERD force fields are described by harmonic potentials:

$$U_{\text{bend}} = \frac{k_\theta(\theta - \theta_0)^2}{2} \quad (2)$$

where $0^\circ \le \theta \le 180^\circ$ is the bond angle and θ_0 and k_θ are constants (see Table 1). The flexible bond lengths in the NERD force field are also described by a harmonic potential:

$$U_{\text{stretch}} = \frac{k_s(l - l_0)^2}{2} \quad (3)$$

where l is the bond length and l_0 and k_s are constants.

All three force fields use the Lennard–Jones 12–6 potential to calculate non-bonded intermolecular energies:

$$U_{\text{LJ}}(r_{ij}) = \begin{cases} 4\varepsilon_{ij}\left[\left(\dfrac{\sigma_{ij}}{r_{ij}}\right)^{12} - \left(\dfrac{\sigma_{ij}}{r_{ij}}\right)^{6}\right], & r_{ij} \le R_{\text{CUT}}, \\ 0, & r_{ij} \ge R_{\text{CUT}} \end{cases} \quad (4)$$

where r_{ij} is the distance between interaction sites i and j, R_{CUT} the cut-off radius, and σ_{ij} and ε_{ij} are the Lennard–Jones size and energy parameters, respectively. The parameters for interactions between like sites are denoted as σ_{ii} and ε_{ii} and are listed in Table 1. Parameters for interactions between two

Table 1
Force field parameters for the NERD, TraPPE and Spyriouni et al. (SA1) force fields

Non-bonded interactions

NERD

$\varepsilon_{CH_3(sp^3)}/k_B = 100.6\,K$ (ethane), $\sigma_{CH_3(sp^3)} = 3.825\,\AA$ (ethane); $\varepsilon_{CH_3(sp^3)}/k_B = 100.0\,K$, $\sigma_{CH_3(sp^3)} = 3.85\,\AA$, $\varepsilon_{CH_2(sp^2)}/k_B = 92.5\,K$, $\sigma_{CH_2(sp^2)} = 3.72\,\AA$, $\varepsilon_{CH(sp^2)}/k_B = 46.0\,K$, $\sigma_{CH(sp^2)} = 3.77\,\AA$ (propene)

Molecules with more than three carbons

$\varepsilon_{CH_3(sp^3)}/k_B = 104.0\,K$, $\sigma_{CH_3(sp^3)} = 3.91\,\AA$, $\varepsilon_{CH_2(sp^3)}/k_B = 45.8\,K$, $\sigma_{CH_2(sp^3)} = 3.93\,\AA$, $\varepsilon_{CH_2(sp^2)}/k_B = 92.5\,K$, $\sigma_{CH_2(sp^2)} = 3.72\,\AA$, $\varepsilon_{CH(sp^2)}/k_B = 46.0\,K$, $\sigma_{CH(sp^2)} = 3.77\,\AA$

TraPPE

$\varepsilon_{CH_3(sp^3)}/k_B = 98.0\,K$, $\sigma_{CH_3(sp^3)} = 3.75\,\AA$, $\varepsilon_{CH_2(sp^3)}/k_B = 46.0\,K$, $\sigma_{CH_2(sp^3)} = 3.95\,\AA$, $\varepsilon_{CH_2(sp^2)}/k_B = 85.0\,K$, $\sigma_{CH_2(sp^2)} = 3.675\,\AA$, $\varepsilon_{CH(sp^2)}/k_B = 47.0\,K$,$\sigma_{CH(sp^2)} = 3.73\,\AA$

SA1

$\varepsilon_{CH_3(sp^3)}/k_B = \varepsilon_{CH_2(sp^3)}/k_B = 47.66\,K$, $\varepsilon_{CH(sp^2)}/k_B = 81.69\,K$, $\sigma_{CH_3(sp^3)} = \sigma_{CH_2(sp^3)} = \sigma_{CH(sp^2)} = 3.915\,\AA$, $\varepsilon_{CH_2(sp^2)}/k_B = 89.93\,K$,$\sigma_{CH_2(sp^2)} = 3.905\,\AA$

Bond lengths

NERD

$k_s/k_B = 96\,500\,K/Å^2$ (C—C, C═C); $l_0 = 1.54$ Å (C—C); $l_0 = 1.33$ Å (C═C)

TraPPE

$k_s/k_B = 0\,K/Å^2$ (C—C, C═C); $l_0 = 1.54$ Å (C—C); $l_0 = 1.33$ Å(C═C)

SA1

$k_s/k_B = 0\,K/Å^2$ (C—C, C═C); $l_0 = 1.53$ Å (C—C); $l_0 = 1.331$ Å(C═C)

Bond angles

NERD

$k_\theta/k_B = 96\,500\,K/deg^2$ (C—C—C, C—C═C); $\theta_0 = 114.0^\circ$ (C—C—C); $\theta_0 = 124.0^\circ$ (C—C═C)

TraPPE

$k_\theta/k_B = 62\,500\,K/deg^2$ (C—C—C); $\theta_0 = 114.0^\circ$(C—C—C)

$k_\theta/k_B = 70\,420\,K/deg^2$ (C—C═C); $\theta_0 = 119.7^\circ$(C—C═C)

SA1

$k_\theta/k_B = 0\,K/deg^2$ (C—C═C, C—C—C); $\theta_0 = 112.0^\circ$ (C—C—C); $\theta_0 = 124.0^\circ$ (C—C═C)

Torsions

NERD

$c_0/k_B = 0\,K$; $c_1/k_B = 355.04\,K$; $c_2/k_B = -68.19\,K$; $c_3/k_B = 791.32\,K$ (C—C—C—C)

$c_0/k_B = 47.97\,K$; $c_1/k_B = 86.31\,K$; $c_2/k_B = -109.71\,K$; $c_3/k_B = 282.08\,K$ (C—C—C═C)

TraPPE

$c_0/k_B = 0\,K$; $c_1/k_B = 355.03\,K$; $c_2/k_B = -68.19\,K$; $c_3/k_B = 791.32\,K$ (C—C—C—C)

$c_0/k_B = 688.5\,K$; $c_1/k_B = 86.36\,K$; $c_2/k_B = -109.77\,K$; $c_3/k_B = 282.24\,K$ (C—C—C═C)

SA1

$c_0/k_B = 0\,K$; $c_1/k_B = 355.03\,K$; $c_2/k_B = -68.19\,K$; $c_3/k_B = 791.32\,K$ (C—C—C—C)

$c_0/k_B = 685.96\,K$; $c_1/k_B = 86.31\,K$; $c_2/k_B = -109.71\,K$; $c_3/k_B = 282.08\,K$ (C—C—C═C)

sites of different types (e.g., between $-CH_3$ and $-CH_2-$) are calculated using the Lorentz–Berthelot mixing rules:

$$\varepsilon_{ij} = \sqrt{\varepsilon_{ii}\varepsilon_{jj}}, \qquad \sigma_{ij} = \frac{\sigma_{ii} + \sigma_{jj}}{2} \tag{5}$$

The NERD and TraPPE force fields use the Lennard–Jones potential expression of Eq. (4) to calculate the potential energy of non-bonded interactions within a specified cut-off radius of 13.8 and 14 Å, respectively [12,17]. For the SA1 force field, the Lennard–Jones potential is used to calculate intermolecular interactions within a first cut-off radius of $1.45\sigma_{ij}$, whereas a quintic spline is used between $1.45\sigma_{ij}$ and $2.30\sigma_{ij}$ [20,44]. For all force fields, analytical tail corrections are applied to estimate the long-range interactions arising from intermolecular separations greater than R_{CUT} [46].

2.1. Simulation methods

The configurational-bias Monte Carlo (CBMC) method was used in conjunction with the Gibbs ensemble Monte

Carlo (GEMC) technique to simulate the four pressure–composition phase diagrams and the temperature–composition phase diagram presented below. In the CBMC algorithm a chain molecule is grown segment by segment using different trial directions for each of the segments. The selection of trial segments is biased in such a way that chains with favourable interactions are generated. This bias is removed exactly in the acceptance/rejection rules. The NVT version of the Gibbs ensemble was used to simulate the two pure component compositions of each of the phase diagrams while the NPT version of the Gibbs ensemble was used to simulate six intermediate compositions for each of the phase diagrams. The intermediate compositions used were 0.1, 0.2, 0.4, 0.6, 0.8 and 0.9 mole fraction of component 1. The total number of molecules used for each of the phase diagrams were as follows: 800 molecules for ethane + propene; 600 molecules for propene + 1-butene; 600 molecules for 1-butene + 1-hexene; 350 molecules for 1-hexene + *n*-octane; and 150 molecules for *n*-dodecane + 1-octadecene.

The types of moves performed during a simulation were: (1) volume changes; (2) molecule identity changes using CBMC [22] and exchanges of molecules between simulation boxes; (3) full regrowing of chains and partial regrowing of chains using CBMC; (4) translation of the centre of mass (COM); and (5) rotation around the COM. Each of the moves was selected at random [47] and were performed with the following fixed probabilities: p_1:p_2:p_3:p_4:p_5 = 0.006:0.328:0.222:0.222:0.222, where p_1 refers the fixed probability of attempting a move of type 1, i.e. a volume change [4]. The maximum volume, translation and rotational displacements were chosen in such a way that 50% of each of these moves was accepted.

All the NVT GEMC Ensemble pure component simulations were equilibrated for at least 100,000 cycles while the NPT GEMC mixture simulations were equilibrated for at least 150,000 cycles (a cycle consists of N attempted moves to the system where N is the total number of molecules in the simulation). Care was taken to ensure that the systems had reached equilibrium before production cycles for ensemble averages were started. The standard deviations of ensemble averages were estimated by dividing the production cycles of each run into five blocks and calculating the standard deviation from the averages obtained from each of these five blocks.

To increase simulation efficiency, multiple trial sites were chosen for the first segment of the chain [48]. This ranged from four for the ethane + propene mixture, which had the shortest chains, to 15 for the *n*-dodecane + 1-octadecene mixture which had the longest chains. Also, a COM-based cut-off was used for the computation of intermolecular forces [12]. In this time-saving approach for the interaction between sites on two different molecules A and B, the periodic image of a bead on B second molecule is evaluated as the same as the periodic image of the COM of B if the distance between the COMs of A and B is less than $d_{COM}(A) + d_{COM}(B) + r_{CUT}$,

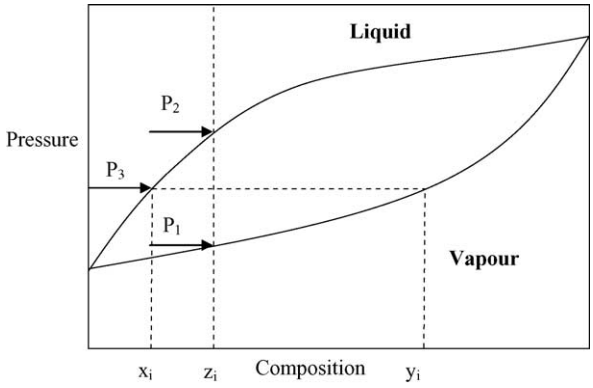

Fig. 1. Example of a *P–x–y* phase diagram at constant temperature.

where $d_{COM}(A)$ is the largest distance between the bead furthest from the COM of A and r_{CUT} the cut-off radius. This also increased computational efficiency by reducing the calculation of periodic images of interactions sites for those interaction sites with the same periodic image as the COM of the molecule without compromising accuracy. Finally, the dual-cut-off CBMC algorithm of Vlugt et al. [49] was used for split energy moves with an inner cut-off distance of 4.5 Å. This was then corrected to the full potential with tail corrections in the acceptance rule.

It is important to choose initial volumes and molecule numbers that do not differ drastically from the eventual equilibrium values. It was observed that choosing values for the initial volumes or initial compositions of the two boxes that differed considerably from the ultimate equilibrium values considerably increased the computational time required for reaching equilibrium.

Another difficulty concerns how one chooses the pressure at which to run an NPT simulation for a binary mixture. The problem associated with the selection of initial conditions is illustrated in Fig. 1. For a given overall mole fraction z_i of component i, only an overall system pressure between P_1 and P_2 will yield a vapour phase in equilibrium with a liquid phase. If the pressure is higher than P_2 then both simulation boxes will revert to equilibrium phases of liquid density whereas if the overall system pressure is chosen below P_1 then both boxes will revert to equilibrium phases of vapour density. An overall system pressure P_3 intermediate between P_1 and P_2 needs to be selected such that an overall mole fraction z_i will yield a liquid mole fraction x_i of component i and a vapour mole fraction y_i of component i. Accurately selecting this pressure P_3 can be quite difficult particularly for narrow phase envelopes, for infinitely dilute regions and for compositions near azeotropes. This difficulty remains even if the constant total volume (i.e. the NVT) Gibbs ensemble is used to simulate the mixture because one would then be required to judiciously select an overall volume that would yield an overall system pressure between P_1 and P_2 at equilibrium.

A simple strategy to partially overcome this problem is to use the experimental pure component densities and the experimental compositions as input parameters to determine the

initial volumes and initial compositions. The aim, however, was to use the NPT simulations to predict the vapour–liquid equilibrium curves without a priori knowledge of equilibrium compositions. A means to reasonably estimate the equilibrium compositions with a minimum of information was thus required.

Since the *n*-alkane and 1-alkene mixtures selected are almost ideal, it was decided to use Raoult's law to estimate the initial compositions. In terms of this very simple description of phase behaviour, the only two inputs required are the pure component saturated vapour pressures which yield an estimate for the vapour and liquid compositions. With the assumption that the molar volumes are linearly additive, it was then possible to estimate reasonable values for the initial molecule numbers and box volumes for the simulations. Using this approach, suitable initial conditions could be set. The NPT GEMC simulation pressure was then adjusted so that at least 10% of the total number of molecules was in the vapour at equilibrium.

There are several other simulation methods that could be employed. These include histogram reweighting techniques [50,51], pseudo-ensembles [52–54], the reaction Gibbs ensemble Monte Carlo [37,55] and the *bubble point ensemble* (BPE) [56,57].

While histogram reweighting performs well for simulations close to the critical point and for pure components, the number of overlapping histograms required for simulation of even a binary system makes the method less advantageous for mixtures. As regards pseudo-ensembles (of which histogram reweighting is an infinite order pseudo-ensemble [52]), Ungerer et al. [56] has pointed out that an iterative scheme requiring repeated chemical potential evaluations is required when using these methods. Pseudo-ensemble methods can therefore also be quite computationally demanding since reasonably accurate chemical potential values are required to obtain satisfactory convergence.

Recently, a method for the direct calculation of bubble points has been proposed by Ungerer et al. [56] and has been extended to the simulation of binary alkane mixtures [57]. This bubble point ensemble method has the advantage over conventional pseudo-ensemble methods in the sense that the coexisting phases remain mechanically coupled. Simulations using the BPE allows for the determination of bubble points by using a fixed liquid composition where the pressure is no longer imposed but rather calculated as an ensemble average. While this method does offer certain advantages over conventional Gibbs ensemble simulations, a very accurate value for the chemical potential is still required. In addition, the authors mentioned problems with vapour condensation arising from larger vapour density fluctuations [56].

The reaction Gibbs ensemble Monte Carlo (RGEMC) has been proposed as a method to more accurately model vapour–liquid phase equilibrium [37,55]. This method has been shown to improve the general location of simulated phase diagrams. In Appendix A it is shown that there will in general also be a shift in the true molar composition. A direct scaling methodology applying the Gamma/Phi approach to VLE [58] is also presented which allows one to generate equivalent RGEMC results from conventional GEMC data.

Since the only major problem when using the NPT Gibbs ensemble is that the system pressure requires fine tuning before beginning a production run, the NPT version of the Gibbs ensemble was used for the mixture simulations.

3. Results and discussion

3.1. Transferability of the SA1 force field parameters to n-alkanes

Whereas the NERD and TraPPE force fields were used to simulate all mixtures studied, the SA1 force field was only used to simulate the 1-butene + 1-hexene and propene + 1-butene mixtures. Although the SA1 force field was parameterized to simulate the pure component properties of 1-alkenes only, we attempted to simulate the *n*-alkane mixtures using the relevant functional group parameters from the SA1 force field parameters. It was found, however, that the SA1 force field is not suitable for simulating the *n*-alkane + 1-alkene mixtures. This is because the sp^3 hybridized $-CH_2-$ and $-CH_3$ functional group parameters in the SA1 force field are not transferable to *n*-alkanes (unlike the NERD and TraPPE force fields). For example, the simulation of pure 1-hexene and pure *n*-octane using the SA1 sp^3 hybridized $-CH_2-$ and $-CH_3$ parameters for the *n*-alkanes incorrectly predicted *n*-octane (simulated saturated vapour pressure of 90.2 kPa at 328.15 K) to be more volatile than 1-hexene (simulated saturated vapour pressure of 85.1 kPa at 328.15 K). No attempt was made to simulate the ethane + propene mixture using the SA1 force field since it was expected that the simulated saturated vapour pressure for ethane would have been significantly worse than for the longer *n*-octane molecule discussed above.

In contrast to the poor transferability of the SA1 parameters to the *n*-alkane chains discussed above, preliminary results indicate that these parameters are transferable to the simulation of long 1-alkene molecules. A plot of the logarithm of the saturated vapour pressure as a function of inverse temperature for 1-octadecene is given in Fig. 2. There is good agreement with the available experimental data [40]. The simulations for 1-octadecene using the NERD and TraPPE force fields are also included in Fig. 2 and show similarly good agreement. Simulated coexistence liquid and vapour densities are shown in Fig. 3 for the NERD, TraPPE and SA1 force fields. The critical temperature for 1-octadecene from the simulations was estimated using a density scaling law [60] while the critical density was estimated using the law of rectilinear diameters [61]. The estimated critical density for 1-octadecene of 0.227, 0.221 and 0.224 g/cm^3 for the NERD, TraPPE and SA1 force fields, respectively, all

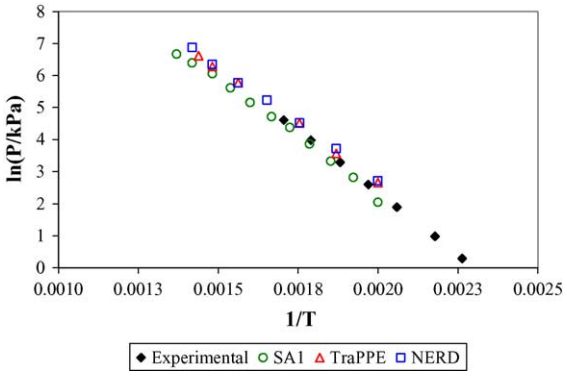

Fig. 2. Vapour pressure for 1-octadecene as predicted by the TraPPE, NERD and SA1 force fields and the experimental 1-octadecene vapour pressure curve [40].

compare favourably with the extrapolated critical density of 0.227 g/cm^3 of Wakeham et al. [62]. However, while the estimated critical temperatures of 744 and 742 K for the NERD and TraPPE force fields, respectively, are in reasonable agreement with the experimental value of 748 K determined by Nitikin and Popov using a pulse-heating technique [63], the estimated critical temperature for 1-octadecene from the SA1 force field off 777 K is in substantial disagreement with the experimental value. It should be noted that the SA1 force field also does not reproduce the experimental saturated liquid and vapour densities well for the short 1-alkenes [20], while good agreement between the NERD and TraPPE force fields was found for critical temperatures and critical densities of the short 1-alkenes [15,19].

No additional parameters were required for the simulation of 1-octadecene for any of these united-atom force fields but additional intramolecular parameters are required when extending these force fields to other homologous series for chemicals with sp^2 hybridized double bonds, e.g. the TraPPE force field has been extended to the simulation of aromatic compounds including benzene [15].

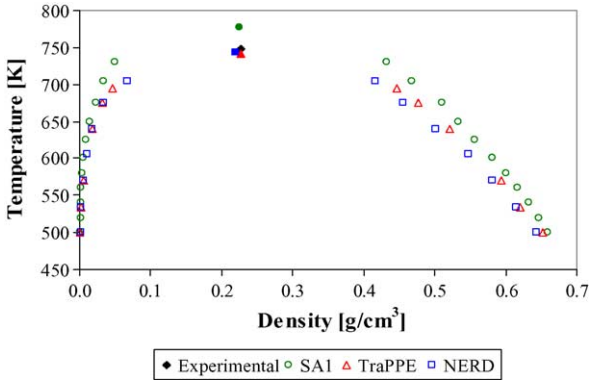

Fig. 3. Simulated pure component coexistence densities for 1-octadecene from the NERD, TraPPE and SA1 force fields and the critical data of Wakeham et al. [62] and Nitikin and Popov [63].

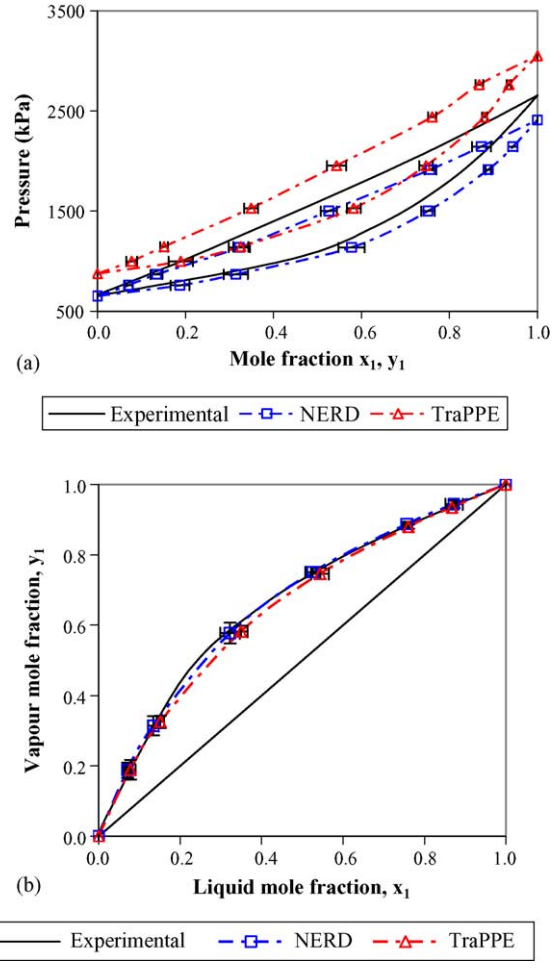

Fig. 4. (a) Simulated *P–x–y* diagrams for ethane (1) + propene (2) at 277.6 K and the corresponding experimental VLE [39]. (b) Simulated *x–y* diagrams for ethane (1) + propene (2) at 277.6 K and the corresponding experimental *x–y* data [39].

3.2. *n*-Alkane + 1-alkene mixtures

The *P–x–y* and *x–y* diagrams for the ethane + propene mixture are shown in Fig. 4. It is important to note that the connecting lines in Fig. 4 are only included to show the trends in the data. It is clear from the *P–x–y* diagram that the TraPPE force field overestimates the experimental phase envelope. This is a direct consequence of the feature that the TraPPE force field overestimates pure component saturated vapour pressures [12,15]. The reason for this is that the TraPPE parameters were parameterized with the initial intent of reproducing all coexistence properties but eventually the authors settled on selecting experimental liquid coexistence densities, critical temperatures and critical densities only as the primary parameterization criteria [12]. In particular, the simulated ethane saturated vapour pressure overestimates the experimental value of 664.7 kPa by 15% and the simulated propene saturated vapour pressure overestimates the experimental value of 2410 kPa by 32% [39]. This results in a

simulated ethane + propene phase envelope that is shifted to higher pressures.

In contrast to the TraPPE force field results, the NERD force field yields an ethane + propene phase envelope that is shifted to lower pressures compared to experimentally measured data. Indeed, the simulated saturated vapour pressures of ethane and propene are lower than the corresponding experimental values by 9.2 and 2.1%, respectively. As for the TraPPE results, this discrepancy between the simulated results and the experimental data may be because the NERD parameters were not fitted to experimental saturated vapour pressures, but rather the Lennard–Jones parameters were primarily parameterized to reproduce experimental coexistence liquid densities, critical temperatures and critical densities as well as experimental second virial coefficients for short hydrocarbon chains (e.g. ethane, ethene, propane and propene). Both force fields, however, yield an isotherm that has the correct shape. This is confirmed by the *x*–*y* plot in Fig. 4b which shows that both the TraPPE and NERD force fields reproduce the experimental *x*–*y* plot to within the statistical deviation of the simulation results. Error bars are included on the *P*–*x*–*y* and *x*–*y* diagrams for this mixture only, and are omitted from the remaining phase diagrams for the sake of clarity. The relative errors are, however, similar (less than ±0.025 mole fraction) for all of the mixtures studied.

The *P*–*x*–*y* and *x*–*y* diagrams for the 1-hexene + *n*-octane mixture at 328.2 K are shown in Fig. 5. As for the ethane + propene mixture, the TraPPE force field overestimates the experimental phase envelope. The experimental *n*-octane saturated vapour pressure of 8.4 kPa [38] is overestimated in the simulations by 58% and that of 1-hexene of 76.8 kPa [38] is overestimated by 43%. However, in contrast to the ethane + propene mixture, the NERD force field also overestimates the experimental phase envelope. The simulated *n*-octane saturated vapour pressure (obtained from the NERD force field) is overestimated in the simulations by 16% and that of 1-hexene by 15%. Similar to the data in Fig. 4b, the simulated *x*–*y* diagrams for the NERD and TraPPE force fields agree with the experimental data in spite of the deviations in the *P*–*x*–*y* data.

As seen in Fig. 6a, the phase envelope for the isobars of *n*-dodecane + 1-octadecene at 760 mmHg obtained from the NERD and TraPPE force fields are shifted to lower temperatures compared to experimental data. This observation is consistent with the trend that both force fields overestimate the pure component saturated vapour pressures for the longer *n*-alkane and 1-alkene chains [12,15,17,19]. Indeed, the experimental normal boiling points of both 1-octadecene and *n*-dodecane of 587.3 and 488.8 K, respectively [40] are underestimated in simulations by both force fields by approximately 10 K. As in the case of the two mixtures discussed before, both force fields yield *x*–*y* data in good agreement with experiment data (Fig. 6b).

Comparison of the simulated data in Fig. 6a with those in Figs. 4a and 5a reveals that the difference between the *T*–*x*–*y* results obtained from the NERD and TraPPE force fields is far smaller for the *n*-dodecane + 1-octadecene mixture than for the ethane + propene and 1-hexene + *n*-octane mixtures. It thus appears that the NERD and TraPPE force fields yield the most similar results for mixtures comprised of longer alkane and 1-alkene molecules. This is to be expected since, once the $-CH_3$ group had been parameterized for ethane, the $-CH_2-$ groups in the TraPPE force field were parameterized for all *n*-alkanes based on a fit to the vapour–liquid coexistence curve of *n*-octane [12]. A similar procedure was adopted for the 1-alkene sp^2 hybridized groups [15]. In contrast to TraPPE, the NERD force field uses a larger parameter set to describe the *n*-alkane and 1-alkene homologous series and thus only assumes functional group transferability for chain lengths of four carbon units and longer [17,19]. With increasing chain length, however, the number of sp^3 hybridized $-CH_2-$ groups dominates the intermolecular Lennard–Jones interactions. Since the Lennard–Jones size and energy parameters for the NERD and TraPPE models for this functional group are very similar (see Table 1), these force fields yield

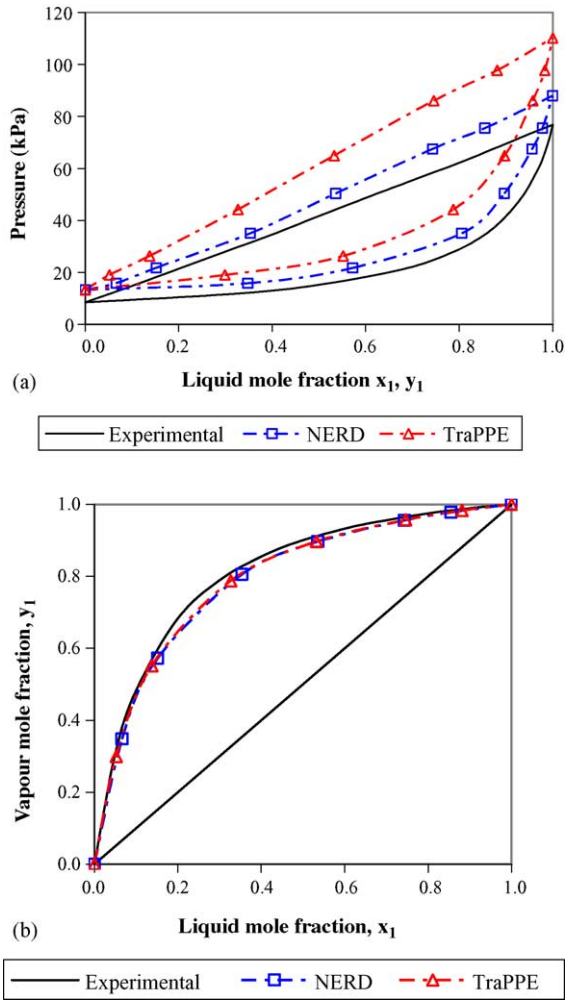

Fig. 5. (a) Simulated *P*–*x*–*y* diagrams for 1-hexene (1) + *n*-octane (2) at 328.15 K and the corresponding experimental VLE [38]. (b) Simulated *x*–*y* diagrams for 1-hexene (1) + *n*-octane (2) at 328.15 K and the corresponding experimental *x*–*y* data [38].

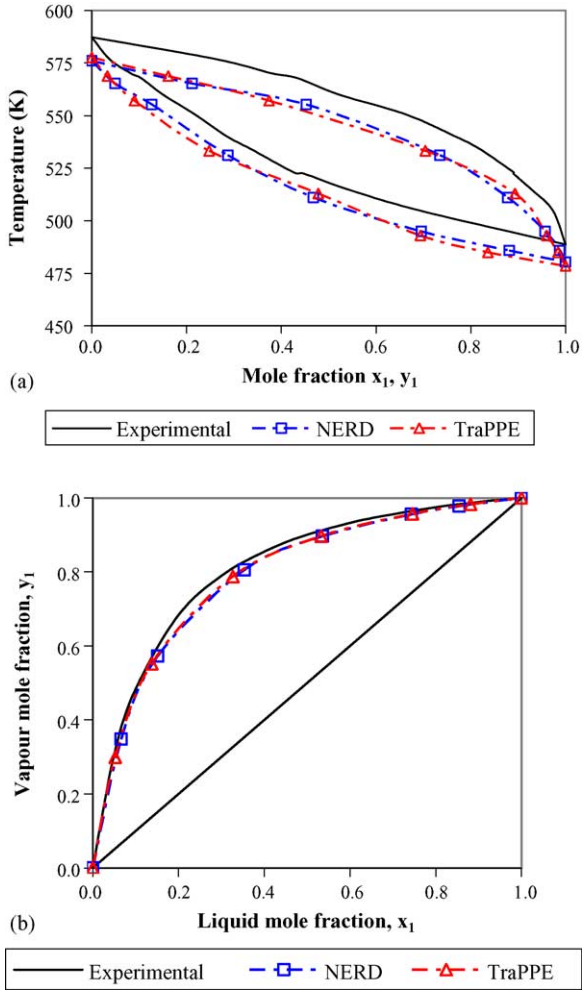

Fig. 6. (a) Simulated *T–x–y* diagrams for *n*-dodecane (1) + 1-octadecene (2) at 760 mmHg and the corresponding experimental VLE [40]. (b) Simulated *x–y* diagrams for *n*-dodecane (1) + 1-octadecene (2) at 760 mmHg and the corresponding experimental *x–y* data [40].

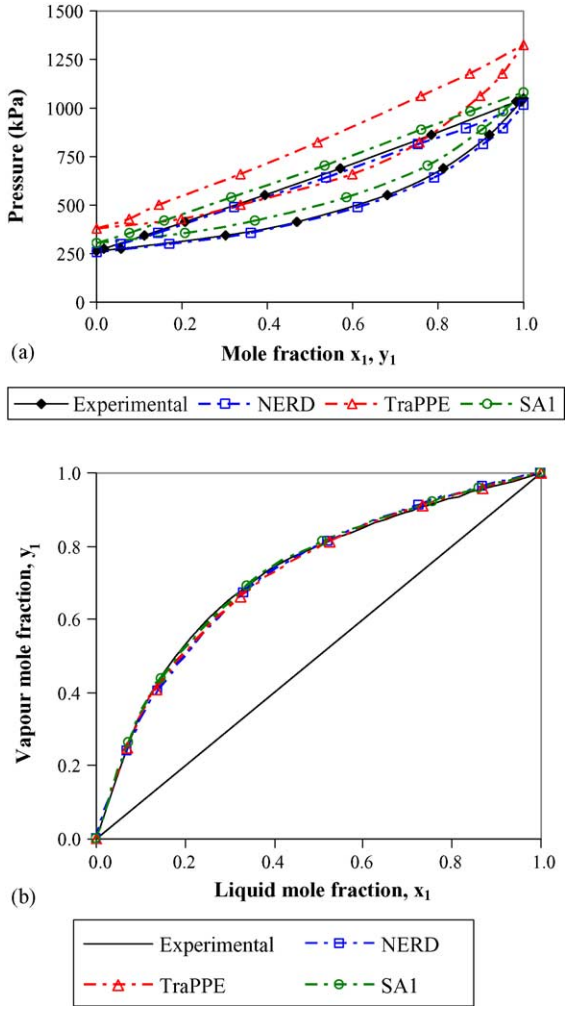

Fig. 7. (a) Simulated *P–x–y* diagrams for propene (1) + 1-butene (2) at 294.3 K and the corresponding experimental VLE [42]. (b) Simulated *x–y* diagrams for propene (1) + 1-butene (2) at 294.3 K and the corresponding experimental *x–y* data [42].

increasingly similar phase diagrams for longer alkane and 1-alkene chains.

3.3. 1-Alkene + 1-alkene mixtures

It is of interest to ascertain if the SA1 force field yields *P–x–y* data that is in better agreement with experiment than the data from the NERD and TraPPE simulations, and if this force field also yields simulated *x–y* results in good agreement with experimentally measured data. As pointed out by Nath et al. [19], the available binary VLE data for 1-alkene mixtures are more limited than for *n*-alkanes. For this reason we were constrained to use the almost ideal mixtures of propene + 1-butene at 294.3 K and 1-butene + 1-hexene at 373 K.

The simulated *P–x–y* and *x–y* diagrams for the propene + 1-butene mixture at 294.3 K are shown in Fig. 7. As for the alkane + 1-alkene mixtures discussed above, the phase envelope obtained from the TraPPE force field is shifted to higher pressures compared to experiment data (the experimental saturated vapour pressure of 1-butene of 263.4 kPa [42] is overestimated by 44%, and that of propene of 1049 kPa [42] is overestimated by 26%). The NERD force field yields a phase envelope in very good agreement with experimentally measured data, although it slightly underestimates the experimental data (the simulations underestimate the experimental saturated vapour pressure of 1-butene by 2% and that of propene by 3%). The SA1 force field also yields data in good agreement with the experimental *P–x–y* data, although the experimental saturated vapour pressure of 1-butene is overestimated by 15% and that of propene by 3%. This is what results in the slight overestimation of the phase envelope shown in Fig. 7a. Thus, even though the SA1 force field is parameterized to reproduce pure component saturated vapour pressures, it yields a 1-butene saturated vapour pressure that is higher than experiment values. However, 1-butene was the shortest 1-alkene used in the parameterization of the SA1 Lennard–Jones terms and no distinction is made between the sp^3 hybridized $-CH_2-$ and $-CH_3$ functional group

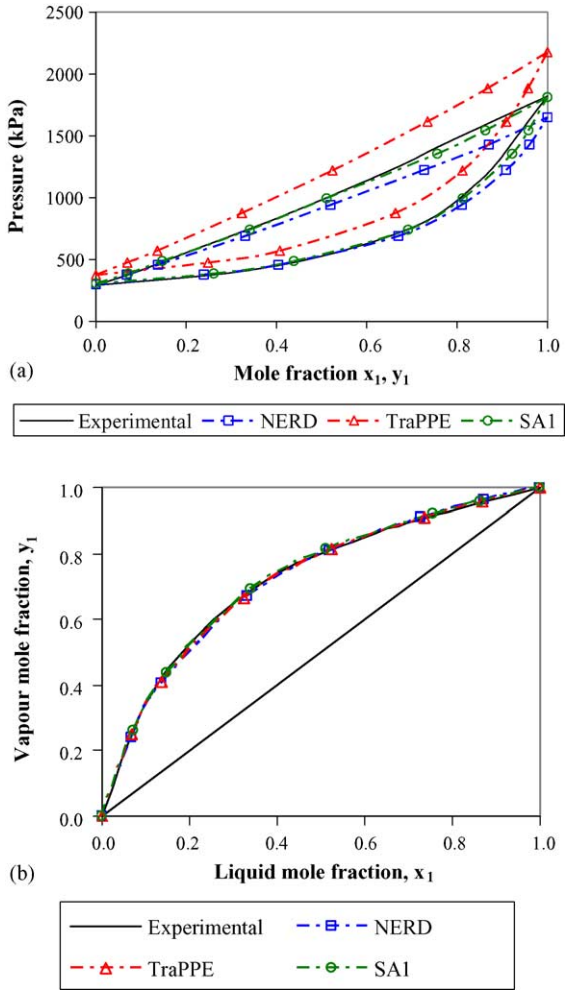

Fig. 8. (a) Simulated *P–x–y* diagrams for 1-butene (1) + 1-hexene (2) at 373 K and the corresponding experimental VLE [41]. (b) Simulated *x–y* diagrams for 1-butene (1) + 1-hexene (2) at 373 K and the corresponding experimental *x–y* data [41].

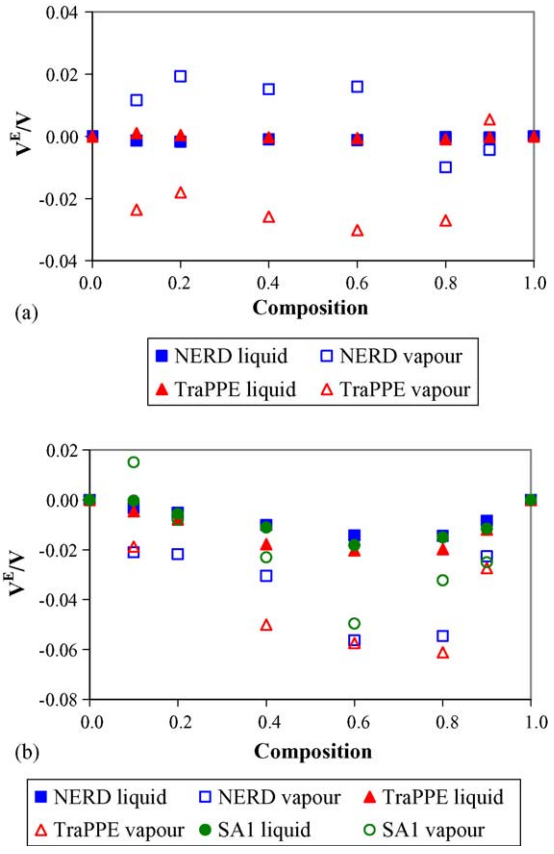

Fig. 9. (a) Plot of the ratio of the excess to the real volumes for both liquid and vapour phases for the 1-hexene + *n*-octane at 328.15 K. (b) Plot of the ratio of the excess to the real volumes for both liquid and vapour phases for the 1-butene + 1-hexene system at 373 K.

parameters (see Table 1). All three force fields reproduce the experimental *x–y* diagram, as was found for the alkane + 1-alkene mixtures discussed earlier.

The *P–x–y* and *x–y* diagrams for 1-butene + 1-hexene at 373 K are shown in Fig. 8. Similar trends to those observed for the propene + 1-butene mixture are seen here. The TraPPE force field overestimates the phase envelope, with the experimental 1-butene and 1-hexene pure component saturated vapour pressures of 1822 and 292.6 kPa being overestimated by 19 and 29%, respectively [41]. The NERD force field underestimates the 1-butene pure component saturated vapour pressure by 9% while the 1-hexene saturated vapour pressure is overestimated by 2%. The *P–x–y* envelope obtained from the NERD force field is thus in good agreement with experiment data. The SA1 force field yields *P–x–y* data that is in best agreement with experimental phase equilibria. For this force field the experimental pure component saturated vapour pressures of 1-hexene and 1-butene are overestimated by only 5 and 0.5%, respectively. Once again, in spite of the deviations in some of the *P–x–y* data, all force fields yield *x–y* diagrams that are in good agreement with the experimental data.

It is interesting to note that the NERD force field underestimates the pure component vapour pressure for some mixtures and overestimates the pure component vapour pressure for other mixtures. The TraPPE force field, however, consistently overestimates the pure component vapour pressure. This possibly indicates that the accuracy of the simulated vapour pressure from the NERD force field may depend on either the chain length or on the reduced temperature of the simulation.

In summary, for both sets of alkane + 1-alkene and 1-alkene + 1-alkene mixtures where both components are short chains the NERD force field yields *P–x–y* data that are in better agreement with experiment than the TraPPE data (Figs. 4, 5, 7 and 8). However, as discussed with reference to the *n*-dodecane + 1-octadecene phase diagram shown in Fig. 6, the TraPPE and NERD force fields yield similar data for *n*-alkane + 1-alkene mixtures that contain longer chains, and both models underestimate the experimental isotherm. Similarl to the NERD force field, the SA1 potential also yields *P–x–y* data that are in good agreement with the experimental data for 1-alkene + 1-alkene mixtures that contain short chains. Also, in spite of deviations in some simulated *P–x–y*

data from the experimental data, all force fields yield *x–y* data in close agreement with the experimental data for all mixtures studied.

3.4. Ideal solution behaviour of the mixtures studied

Fig. 9 shows plots of the relative excess volumes of the liquid and vapour phases as a function of composition for the 1-hexene + *n*-octane mixture at 328 K and the 1-butene + 1-hexene mixture at 373 K. Similar results were obtained for the other mixtures and are thus not shown here. The data sets are obtained for overall mole fractions of component 1 of 0.0, 0.1, 0.2, 0.4, 0.6, 0.8, 0.9 and 1.0 as one follows a data set from left to right in the figures. The proximity of the data about the $V^E/V = 0$ line confirms the ideal behaviour of the solutions studied and indicates why the method of assuming ideal behaviour for choosing the initial conditions for the simulations worked. The reason for the apparently larger excess volumes of the vapour phase is attributable to the larger deviation which one typically finds for the simulated values for vapour densities and vapour molar volumes.

4. Conclusions

The configurational-bias Monte Carlo method in the Gibbs ensemble, using the NERD, TraPPE and Spyriouni et al. 1-alkene force fields, was used to simulate phase equilibrium data for the ethane + propene, 1-hexene + *n*-octane, *n*-dodecane + 1-octadecene, propene + 1-butene and 1-butene + 1-hexene binary mixtures. It was confirmed that the relevant *n*-alkane parameters from the Spyriouni et al. 1-alkene force field are not transferable to the simulation of *n*-alkanes although it was established that this force field does provide pure component vapour–liquid equilibrium data of 1-alkenes in good agreement with the experimental data. Of the three force fields used, the NERD force field, in general, provides a better description of the *P–x–y* and *T–x–y* phase diagrams although the Spyriouni et al. force field also described the 1-alkene + 1-alkene mixtures well. In addition, the NERD and TraPPE force fields seem to yield increasingly similar results as the length of the hydrocarbon chain increases. This can be attributed to similar values of the Lennard Jones parameters for the $-CH_2-$ functional group in the NERD and TraPPE force fields which dominates the intermolecular interactions for long hydrocarbon chain lengths.

Despite substantial deviation between the simulated and experimental *P–x–y* data for some of the investigated mixtures, all force fields yield *x–y* diagrams in very good agreement with the experimental data for all mixtures studied. Part of the reason for this is that the mixtures investigated are approximately ideal. This is an important result when using simulated data for designing industrial equipment, because it suggests that phase equilibrium data from molecular simulations can potentially provide reliable compositional information for sizing separation vessels and that the industrial use of simulated compositions for mixtures of hydrocarbons is not limited by the need for more sophisticated force fields.

A method, based on using Raoult's law, for identifying reasonable initial conditions for the NPT Gibbs ensemble simulations for approximately ideal mixtures is also presented.

Acknowledgements

The authors would like to acknowledge the use of the BIGMAC Monte Carlo code and the computer expertise provided by Ander Askåsen and Daniel Johansson as well as financial assistance from SIDA (Swedish International Development and Co-operation Agency), the NRF (National Research Fund) and SASOL Ltd.

List of symbols

c_0, c_1, c_2, c_3	torsional constants (J)
f	pure component fugacity (kPa)
k_B	Boltzmann's constant (J/K)
k_s	bond stretching constant (J/Å^2)
k_θ	bond angle bending constant (J/deg^2)
l	bond length (Å)
N	number of molecules of a particular component
P	pressure (kPa)
$P^{L\rightarrow V}$	probability of transferring a molecule from the liquid to the vapour
r	distance between Lennard–Jones interaction sites (Å)
R_{CUT}	intermolecular cut-off radius (Å)
T	temperature (K)
ΔU	energy change of a particular box (J)
V	box volume per molecule (Å^3/molecule)
x	liquid mole fraction
y	vapour mole fraction
z	overall (both phases) mole fraction

Greek letters

γ_i	activity coefficient in the liquid phase of component i
ε	Lennard–Jones energy parameter (J)
θ	bending bond angle (°)
μ	chemical potential (J)
ρ	number density (number of molecules/Å^3)
σ	Lennard–Jones size parameter (Å)
ϕ	torsional angle (rad)
$\hat{\phi}_i$	fugacity coefficient of component i in solution in the vapour
Φ_i	non-ideality correction factor for component i in the vapour

Subscripts

bend	bond angle bending
exp	experimental value
G	vapour
i, j	molecular species or interaction sites

L	liquid
stretch	bond stretching
tors	torsion
0	equilibrium value

Superscripts

E	excess property
sat	saturated property
0	standard property

Appendix A

The RGEMC is able to achieve a shift in the simulated phase diagram by modifying the expression for the chemical potential in the vapour phase as follows [37]:

$$\mu^{\mathrm{G}}_{i,\mathrm{RGEMC}} = \mu^{\mathrm{G},0}_i(T, P^0) + \mu^{\mathrm{G,E}}_{i,\mathrm{GEMC}} + \left\{ k_{\mathrm{B}} T \ln\left(\frac{P^{\mathrm{sat}}_{i,\mathrm{exp}}}{P^{\mathrm{sat}}_{i,\mathrm{GEMC}}} \right) \right\} \tag{6}$$

where μ^{G}_i denotes the chemical potential of species i in the vapour phase, P^{sat}_i the pure component saturated vapour pressure of species i, T the temperature, k_{B} the Boltzmann's constant, $\mu^{\mathrm{G}}_i(T, P^0)$ the standard chemical potential in the ideal gas state, subscript GEMC denotes a value from a Gibbs ensemble simulation, subscript RGEMC a value from a reaction Gibbs ensemble simulation, subscript exp denotes the experimental value and superscript E a residual quantity. The term in curly brackets may be viewed as an 'adjustment' to the reference chemical potential and is accounted for in the acceptance rule for a molecule transfer move in the RGEMC:

$$P^{\mathrm{L}\to\mathrm{G}} = \min\left\{ 1, \frac{P^{\mathrm{sat}}_{i,\mathrm{exp}}}{P^{\mathrm{sat}}_{i,\mathrm{GEMC}}} \frac{N^{\mathrm{L}} V^{\mathrm{G}}}{(N^{\mathrm{G}}+1)V^{\mathrm{L}}} \times \exp\left[-\frac{\Delta U^{\mathrm{L}} + \Delta U^{\mathrm{G}}}{k_{\mathrm{B}} T} \right] \right\} \tag{7}$$

where $P^{\mathrm{L}\to\mathrm{V}}$ is the probability of transferring a molecule from the liquid to the vapour phase, N the number of molecules, V the volume, superscript G denotes the vapour, superscript L the liquid and ΔU the energy change in the liquid or vapour box. The only difference between Eq. (7) and the transition probability for the transfer of a molecule from the liquid to the vapour in the Gibbs ensemble is the presence of the term $P^{\mathrm{sat}}_{i,\mathrm{exp}}/P^{\mathrm{sat}}_{i,\mathrm{GEMC}}$.

An analogous expression to Eq. (6) may also be written for the liquid phase to ensure equality of chemical potentials between the two coexisting phases where the superscript G of Eq. (6) are replaced by superscript L. Unlike in the vapour phase, the adjustment to the reference chemical potential is not accounted for in the acceptance rule of Eq. (7). To understand how this term is accounted for and how the phase diagram is shifted using RGEMC, it is convenient to consider the Gamma/Phi formulation for VLE [58]:

$$y_i \hat{\phi}_i P = x_i \gamma_i f_i \tag{8}$$

or, equivalently,

$$y_i \Phi_i P = x_i \gamma_i P^{\mathrm{sat}}_i, \quad \Phi_i = \frac{\hat{\phi}_i f_i}{P^{\mathrm{sat}}_i} \tag{9}$$

where y_i is the mole fraction of species i in the vapour, x_i the mole fraction of species i in the liquid, P the pressure, P^{sat}_i the saturated pure component vapour pressure of species i, γ_i the activity coefficient species i, f_i the fugacity of component i, $\hat{\phi}_i$ the fugacity coefficient of component i in solution in the vapour and Φ_i measures deviations from ideal behaviour in the vapour. The term on the right-hand side of Eq. (8) is directly related to the chemical potential of the liquid phase. The link between the chemical potentials of a GEMC simulation and a RGEMC simulation may thus be written as

$$(x_i \gamma_i f_i)_{\mathrm{GEMC}} = \exp[(\mu^{\mathrm{L}}_i)_{\mathrm{GEMC}}] = \frac{P^{\mathrm{sat}}_{i,\mathrm{GEMC}}}{P^{\mathrm{sat}}_{i,\mathrm{exp}}} \exp[(\mu^{\mathrm{L}}_i)_{\mathrm{RGEMC}}] \tag{10}$$

Therefore Eq. (8) may be rewritten as follows:

$$(y_i \Phi_i P)_{\mathrm{RGEMC}} = (x_i \gamma_i P^{\mathrm{sat}}_i)_{\mathrm{GEMC}} \left(\frac{P^{\mathrm{sat}}_{i,\mathrm{exp}}}{P^{\mathrm{sat}}_{i,\mathrm{GEMC}}} \right) = (x_i \gamma_i)_{\mathrm{GEMC}} P^{\mathrm{sat}}_{i,\mathrm{exp}} \tag{11}$$

Since the scaling term $(P^{\mathrm{sat}}_{i,\mathrm{GEMC}}/P^{\mathrm{sat}}_{i,\mathrm{exp}})$ represents an additional contribution to the reference chemical potential, both Φ_i and γ_i (which account for non-ideal vapour and liquid deviations, respectively) are not functions of this new contribution. Thus, in general, for a given x_i a necessary condition for both the RGEMC and GEMC to yield similar compositions is that:

$$\frac{P_{\mathrm{RGEMC}}}{P^{\mathrm{sat}}_{i,\mathrm{exp}}} = \left(\frac{P}{P^{\mathrm{sat}}_i} \right)_{\mathrm{GEMC}} \tag{12}$$

where the above relation has been derived by a ratio of Eq. (11) written for both the Gibbs ensemble and for the reaction Gibbs ensemble and where P may be evaluated for a binary mixture from:

$$P = \frac{x_1 \gamma_1 P^{\mathrm{sat}}_1}{\Phi_1} + \frac{x_2 \gamma_2 P^{\mathrm{sat}}_2}{\Phi_2} \tag{13}$$

by using the relation that the mole fractions in the vapour must sum to one. In general, Eq. (12) is not satisfied by the RGMEC methodology unless both of the simulated vapour pressures of the pure components exhibit the same relative deviation from the experimental saturated vapour pressures of the pure components. For all other cases, a given x_i the y_i will not yield identical y_i for both the GEMC and RGEMC.

It is possible to generate the results from RGEMC using standard GEMC by use of the following formulae which may

be derived by using Eqs. (11) and (13) and by substituting the experimental vapour pressures:

$$y_i = x_i \left(\frac{\gamma_i P^{\text{sat}}_{i,\text{exp}}}{\Phi_i} \right)_{\text{GEMC}} \frac{1}{P_{\text{RGEMC}}} \tag{14}$$

$$P_{\text{RGEMC}} = \sum_i \left[\left(\frac{x_i \gamma_i}{\Phi_i} \right)_{\text{GEMC}} P^{\text{sat}}_{i,\text{exp}} \right] \tag{15}$$

where

$$\left(\frac{\gamma_i}{\Phi_i} \right)_{\text{GEMC}} = \left(\frac{y_i P}{x_i P^{\text{sat}}_i} \right)_{\text{GEMC}} \tag{16}$$

and may be evaluated from the GEMC results at the end of a simulation.

In order to demonstrate this procedure we have plotted the original data for the isobutene + MTBE system at 350 K in Fig. 10 [37]. Although there are only three mixture data points, it is seen that the *x*–*y* data calculated from Eqs. (14)–(16) using the results from the Gibbs ensemble simulations lie on the plot for the *x*–*y* data from the reaction Gibbs ensemble simulations and that the vapour mole fractions are shifted from the original Gibbs ensemble results.

A general improvement in the location of a phase diagram predicted by simulation is, however, seen when using RGEMC. The above discussion allows one to assess how much the compositional data is shifted when using RGEMC.

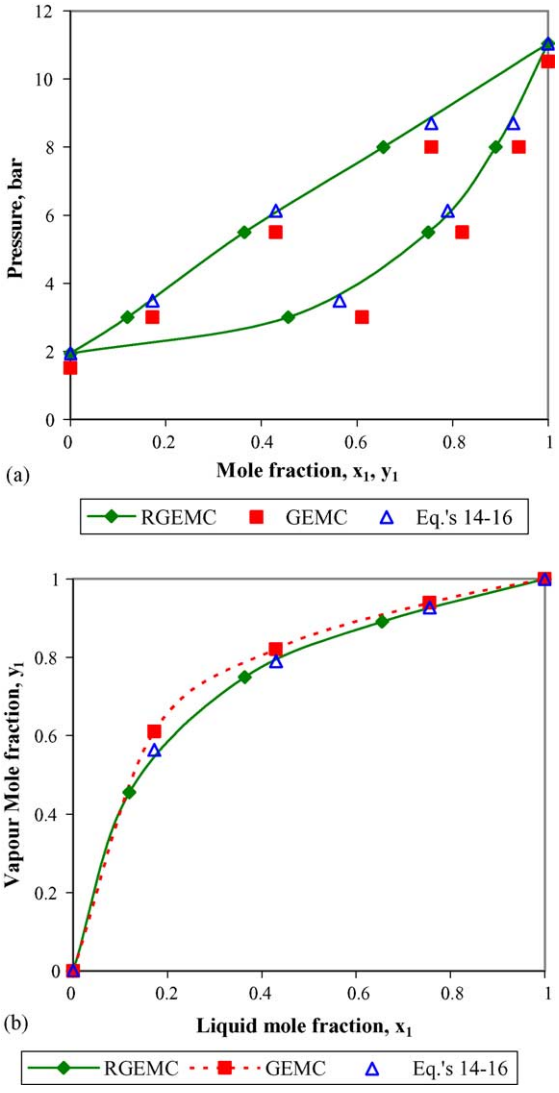

Fig. 10. (a) Simulated *P*–*x*–*y* diagrams for isobutene (1) + MTBE (2) at 350 K from the original RGEMC simulations [37] and using Eqs. (14)–(16). (b) Simulated *x*–*y* diagram for isobutene (1) + MTBE (2) at 350 K from the original RGEMC simulations [37] and using Eqs. (14)–(16).

References

[1] J.D. Raal, A.L. Mühlbauer, Phase Equilibria: Measurement and Computation, Taylor & Francis, Washington, DC, 1998.
[2] A.Z. Panagiotopoulos, J. Phys.: Condens. Mat. 12 (2000) R25–R52.
[3] P. Ungerer, Oil Gas Sci. Technol. 58 (2003) 271–297.
[4] B. Smit, S. Karaborni, J.I. Siepmann, J. Chem. Phys. 102 (1995) 2126–2140.
[5] G.C.A.M. Mooij, D. Frenkel, B. Smit, J. Phys.: Condens. Mat. 4 (1992) L255–L259.
[6] D. Frenkel, G.C.A.M. Mooij, B. Smit, J. Phys.: Condens. Mat. 4 (1992) 3053–3076.
[7] J.J. de Pablo, M. Laso, U.W. Suter, J. Chem. Phys. 96 (1992) 2395–2403.
[8] J.J. de Pablo, M. Laso, U.W. Suter, J. Chem. Phys. 96 (1992) 6157–6162.
[9] A.Z. Panagiotopoulos, Mol. Phys. 61 (1987) 813–826.
[10] A.Z. Panagiotopoulos, Mol. Phys. 63 (1988) 527–545.
[11] B. Smit, P. de Smedt, D. Frenkel, Mol. Phys. 68 (1989) 931–950.
[12] M.G. Martin, J.I. Siepmann, J. Phys. Chem. B 102 (1998) 2569–2577.
[13] M.G. Martin, J.I. Siepmann, J. Phys. Chem. B 103 (1999) 4508–4517.
[14] B. Chen, J.I. Siepmann, J. Phys. Chem. B 103 (1999) 5370–5379.
[15] C.D. Wick, M.G. Martin, J.I. Siepmann, J. Phys. Chem. B 104 (2000) 8008–8016.
[16] B. Chen, J.J. Potoff, J.I. Siepmann, J. Phys. Chem. B 105 (2001) 3093–3104.
[17] S.K. Nath, F.A. Escobedo, J.J. de Pablo, J. Chem. Phys. 108 (1998) 9905–9911.
[18] S.K. Nath, J.J. de Pablo, Mol. Phys. 98 (2000) 231–238.
[19] S.K. Nath, B.J. Banaszak, J.J. de Pablo, J. Chem. Phys. 114 (2001) 3612–3616.
[20] T. Spyriouni, I.G. Economou, D.N. Theodorou, J. Am. Chem. Soc. 121 (1999) 3407–3413.
[21] J.R. Errington, A.Z. Panagiotopoulos, J. Phys. Chem. B 103 (1999) 6314–6322.
[22] M.G. Martin, J.I. Siepmann, J. Am. Chem. Soc. 119 (1997) 8921–8924.
[23] M.G. Martin, J.I. Siepmann, M.R. Schure, J. Phys. Chem. B 103 (1999) 11191–11195.
[24] M.G. Martin, N.D. Zhuravlev, B. Chen, P.W. Carr, J.I. Siepmann, J. Phys. Chem. B 103 (1999) 2977–2980.
[25] M.G. Martin, B. Chen, J.I. Siepmann, J. Phys. Chem. B 104 (2000) 2415–2423.
[26] S.K. Nath, F.A. Escobedo, J.J. de Pablo, I. Patramai, Ind. Eng. Chem. Res. 37 (1998) 3195–3202.
[27] J.J. Potoff, J.R. Errington, A.Z. Panagiotopoulos, Mol. Phys. 97 (1999) 1073–1083.
[28] P. Ungerer, C. Beauvais, J. Delhommelle, A. Boutin, B. Rousseau, A.H. Fuchs, J. Chem. Phys. 112 (2000) 5499–5510.

[29] E. Bourasseau, P. Ungerer, A. Boutin, A.H. Fuchs, Mol. Simul. 28 (2002) 317–336.
[30] E. Bourasseau, M. Haboudou, A. Boutin, A.H. Fuchs, J. Chem. Phys. 118 (2003) 3020–3034.
[31] P. Pascual, P. Ungerer, B. Tavitian, P. Pernot, A. Boutin, Phys. Chem. Chem. Phys. 5 (2003) 3684–3693.
[32] P. Pascual, P. Ungerer, B. Tavitian, P. Pernot, A. Boutin, J. Phys. Chem. B 108 (2004) 393–398.
[33] R.H. Grubbs, S. Chang, Tetrahedron 54 (1998) 4413–4450.
[34] A.M. Rouhi, Chem. Eng. News 80 (51) (2002) 29–33.
[35] S.K. Nath, J.J. de Pablo, J. Phys. Chem. B 103 (1999) 3539–3544.
[36] S.K. Nath, B.J. Banaszak, J.J. de Pablo, Macromolecules 34 (2001) 7841–7848.
[37] M. Lísal, W.R. Smith, I. Nezbeda, J. Phys. Chem. B 103 (1999) 10496–10505.
[38] Dortmund Data Bank Vapour–Liquid Equilibrium Data Compilation, DDBST GmbH, Oldenburg, 1973.
[39] R.A. McKay, H.H. Reamer, B.H. Sage, W.N. Lacey, Ind. Eng. Chem. 43 (1951) 2112–2117.
[40] B.T. Jordan, M. van Winkle, Ind. Eng. Chem. 43 (1951) 2908–2912.
[41] S. Laugier, D. Richon, J. Chem. Eng. Data 41 (1996) 282–284.
[42] G.H. Goff, P.S. Farrington, B.H. Sage, Ind. Eng. Chem. 42 (1952) 735–743.
[43] D. Dubbeldam, S. Calero, T.J.H. Vlugt, R. Krishna, T.L.M. Maesen, B. Smit, J. Phys. Chem. B 33 (2004) 12301–12313.
[44] D.N. Theodorou, U.W. Suter, Macromolecules 18 (1985) 1467–1478.
[45] W.L. Jorgensen, J.D. Madura, C.J. Swenson, J. Am. Chem. Soc. 106 (1984) 6638–6646.
[46] M.P. Allen, D.J. Tildesley, Computer Simulation of Liquids, Oxford University Press, New York, 1987.
[47] B. Smit, D. Frenkel, J. Chem. Phys. 94 (1991) 5663–5668.
[48] K. Esselink, L.D.J.C. Loyens, B. Smit, Phys. Rev. E 51 (1995) 1560–1568.
[49] T.J.H. Vlugt, M.G. Martin, B. Smit, J.I. Siepmann, R. Krishna, Mol. Phys. 94 (1998) 727–733.
[50] A.M. Ferrenberg, R.H. Swendsen, Phys. Rev. Lett. 63 (1989) 1195–1198.
[51] A.Z. Panagiotopoulos, V. Wong, M.A. Floriano, Macromolecules 31 (1998) 912–918.
[52] F.A. Escobedo, J. Chem. Phys. 108 (1998) 8761–8772.
[53] F.A. Escobedo, J. Chem. Phys. 110 (1999) 11999–12010.
[54] F.A. Escobedo, AIChE J. 46 (2000) 2086–2096.
[55] M. Lísal, W.R. Smith, I. Nezbeda, Fluid Phase Equilib. 181 (2001) 127–146.
[56] P. Ungerer, A. Boutin, A.H. Fuchs, Mol. Phys. 97 (1999) 523–539.
[57] P. Ungerer, A. Boutin, A.H. Fuchs, Mol. Phys. 99 (2001) 1423–1434.
[58] J.M. Smith, H.C. Van Ness, M.M. Abbott, Introduction to Chemical Engineering Thermodynamics, 5th ed., McGraw-Hill, Singapore, 1996.
[60] J.S. Rowlinson, B. Widom, Molecular Theory of Capillarity, Oxford University Press, New York, 1989, p. 261.
[61] J.S. Rowlinson, F.L. Swinton, Liquids and Liquid Mixtures, 3rd ed., Butterworths, London, 1982, pp. 70–75.
[62] W.A. Wakeham, G.St. Cholakov, R.P. Stateva, J. Chem. Eng. Data 47 (2002) 559–570.
[63] E.D. Nitikin, A.P. Popov, Fluid Phase Equilib. 166 (1999) 237–243.

Further reading

[59] L.R. Dodd, D.N. Theodorou, Adv. Polym. Sci. 116 (1994) 249–281.